J Mater Sci (2012) 47:6444–6450
DOI 10.1007/s10853-012-6576-y

Effects of macropore size on structural and electrochemical properties of hierarchical porous carbons

Qilin Cheng · Yuming Xia · Vladimir Pavlinek · Yanfang Yan · Chunzhong Li · Petr Saha

Received: 2 January 2012 / Accepted: 11 May 2012 / Published online: 26 May 2012
© Springer Science+Business Media, LLC 2012

Abstract Hierarchical porous carbons (HPCs) were synthesized by a colloid crystal template method with phenolic resin as carbon source and triblock copolymer Pluronic F127 as a soft template. The obtained HPCs with tunable macropore size of 242–420 nm exhibit large BET surface areas ($\sim$900 m^2 g^{-1}) and large pore volumes ($\sim$1.2 cm^3 g^{-1}). With an increase in the diameters of silica template, the BET surface areas and pore volumes of HPCs decrease. The electrochemical properties of the HPCs with various macropore sizes used as supercapacitor electrodes materials were evaluated using cyclic voltammetry, galvanostatic charge–discharge, and electrochemical impedance spectroscopy techniques. The results show the HPC with the macropore size of 242 nm possesses the largest specific capacitance among the HPCs. The excellent capacitive behavior of HPC-242 can be attributed to its faster ion transport behavior and better ion-accessible surface area.

Introduction

Over the past few years, hierarchical porous carbons (HPCs) with three-dimensionally interconnected micro-, meso-, and macroporous network have attracted considerable attention due to their promising applications in catalysis, adsorption, drug delivery, and energy storage [1–4]. In particular, HPCs used for electrode materials in supercapacitors have been the subject of intense studies in recent years. Supercapacitors are well-known energy storage devices which can deliver high power and store remarkable energy [5–10]. To develop an advanced supercapacitor device, an active electrode material with high capacity performance is urgently required. HPC materials would be an appropriate candidate for the fabrication of advanced supercapacitors because they can combine the structural advantages of multi-level pores. It is now widely accepted that the micropores enhance the electric double-layer capacitance, the mesopores provide low-resistant pathway for ions' transport, and the macropores act as ion-buffering reservoirs to decrease the diffusion distance [11–14]. Therefore, high-performance electrode materials with fast ion transport and high charge storage capability could be obtained by the combination of different pores in carbon nanomaterials.

So far, various approaches towards the synthesis of HPC materials have been conducted based on template strategy, which involves filling the void space of a template with carbon sources followed by carbonization under an inert atmosphere and subsequent removal of the template [15–19]. For instance, Cheng and coauthors [16] synthesized 3D HPC material using alkaline system $Ni(OH)_2$/NiO as hard template and it exhibited high energy and power densities in both aqueous ad organic electrolytes. Carbon capsules with hierarchical porous structures were synthesized by Yu and coauthors [17] using a solid core/mesoporous shell silica spheres as a template, and its specific surface area was around 1230 m^2 g^{-1}. However, the mesoporous structure of the obtained porous carbon materials was disordered. In order to achieve better electrochemical capacitance of HPC, a more ordered mesoporous structure

Q. Cheng · Y. Xia · Y. Yan · C. Li
Key Laboratory for Ultrafine Materials of Ministry of Education, School of Materials Science and Engineering, East China University of Science and Technology, Shanghai 200237, China

Q. Cheng (✉) · V. Pavlinek · P. Saha
Centre of Polymer Systems, Polymer Centre, Tomas Bata University in Zlin, Nam. T. G. Masaryka 5555, 760 01 Zlin, Czech Republic
e-mail: chengql@ecust.edu.cn

is desirable. Therefore, some block copolymers were used as a soft template to get uniform mesopores during the preparation of porous carbon. Zhao and coauthors [20] reported the preparation of HPC using silica colloidal crystals and triblock copolymer (Pluronic F127) as a dual template . HPC were also synthesized using poly(methyl methacrylate) or polystyrene instead of silica as template. The formation of macropores and mesopores is attributed to the large silica or polymer hard template and triblock copolymers soft template, respectively, and micropores are formed due to carbonization of polymer. In addition, an effective template-free fabrication of a novel type of HPCs by constructing carbonyl crosslinking bridges between polystyrene chains has also been recently reported by Wu's group [21].

In spite of the fact that there are many studies concerning the design and fabrication of such HPC materials via template or template-free methods, the macropore size which affects the structural and electrochemical properties of HPCs has not been clarified yet. Herein, we report the synthesis of HPCs with various macropore sizes through the control of the size of silica spheres template. The effect of the macropore size on the structural and electrochemical properties of HPCs is investigated to further elucidate the relationship between the pore structure and the electrochemical capacitive behavior of porous carbon materials.

Experimental

Materials

Tetraethyl orthosilicate (TEOS), ethanol, aqueous ammonia (28 %), hydrofluoric acid (HF, 40 %), and F127 (amphiphilic triblock copolymer PEO_{127}–PPO_{70}–PEO_{127}) were purchased from Aldrich. Phenolic resin was obtained from Bengbu Tianyu high temperature material Company, China, and other reagents were used as received without further purification.

Synthesis of HPCs

The HPCs were prepared by impregnating phenol resin and F127 into the void of silica microsphere. The silica microspheres with different diameters (260, 380, and 450 nm) were synthesized according to stöber's method. In a typical synthesis strategy, *X* ml ammonia was added in a mixed solution (7-ml deionized water and 20-ml absolute ethanol) and stirred for 10 min, then 3-ml TEOS and 11-ml absolute ethanol were poured into and stirred for 8 h to form milky white liquid. Subsequently, 0.5 g F127 and 4 g of 20 wt% ethanol solution of phenolic resin were added and stirred for another 24 h, the hybrid system was evaporated for 12 h in a petri dish under room temperature, and followed by further heating to 120 °C for 24 h. Finally, the resulting compound was carbonized under N_2 via heating ramps of 1 °C/min from room temperature to 350 °C and hold for 4 h, and then ramped at 5 °C/min to 800 °C and hold for 2 h. The obtained black powder were treated with 10 wt% HF solution to remove silica template, followed by washing with deionized water and ethanol and dried at 60 °C for 12 h to give HPCs (The particle size of silica spheres is 260, 380, and 450 nm when *X* is 1, 3 and 5, respectively).

Characterization

The morphology and structure of materials were characterized by the filed-emission scanning electron microscope (FE-SEM, JEOL JSM-6700F) and transmission electron microscopy (TEM H-800). Nitrogen adsorption–desorption isotherms were performed with ASAP 2020 Micromeritics analyzer at 77 K and the specific surface areas (S_{BET}) were deduced by using the BET equation. Raman spectra of the powders were collected on a Lab Ram Infinity Raman spectrometer, using 514.5 nm lasers.

Electrochemical measurements

To measure the electrochemical property, a working electrode mixture with 80 wt% active materials, 10 wt% carbon black, and 10 wt% polytetrafluoroethylene (PTFE) were prepared. Then, the mixture was pressed into thin disks with uniform thickness, followed by evaporating the residual water by vacuum-drying at 60 °C for 24 h, and then immersed in 1 mol L^{-1} aqueous H_2SO_4 for 24 h. The mass loading of the active materials on each electrode is about 8 mg cm^{-2}. A symmetric sandwich two-electrode system was used to measure the electrochemical properties. Cyclic voltammeter (CV) and electrochemical impedance (EI) experiments were conducted with a PARSTAT 2273/CS130 electrochemical station; and galvanostatic charge–discharge (CD) curves were performed with LAND CT2001A at room temperature. The potential range for CV, EI and CD examinations varied from −0.2 to 0.8 V.

Results and discussion

Characterization of materials

The monodisperse silica microspheres with diameters of 260, 380, and 450 nm (Fig. 1) are used as the hard template for preparation of HPCs. The macropore size of HPCs are depended on the size of the silica spheres. The morphology

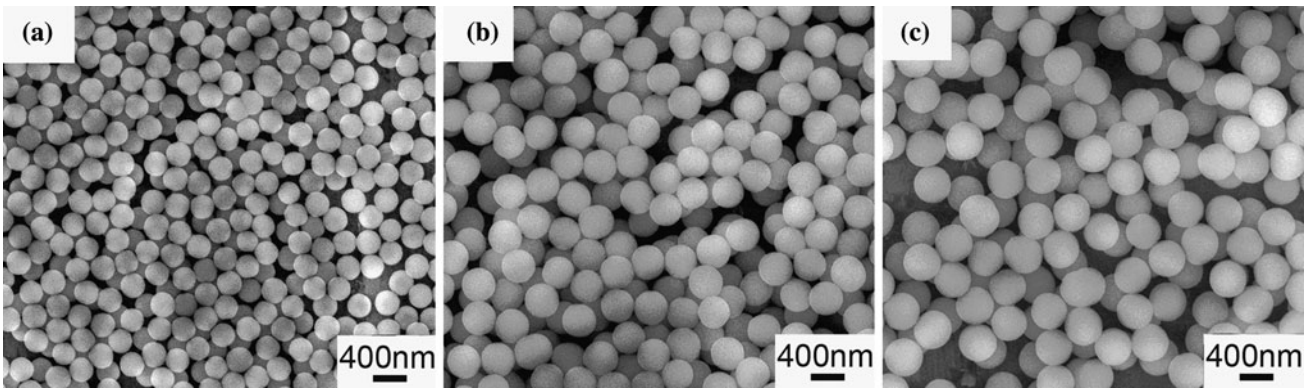

Fig. 1 SEM images of **a** SiO_2-260, **b** SiO_2-380, and **c** SiO_2-450

and structure of the as-prepared HPCs are shown in Fig. 2. As shown in Fig. 2a, c and e, all the HPCs composed of honeycomb-like cavities possess interconnected porous networks, indicating that the 3D macrostructure of the colloid silica crystals is successfully replicated. The mesoporous structures of porous carbons were observed with TEM. Figure 2b, d and f illustrate the TEM images of the HPCs. Ordered mesopores (8–10 nm) formed within the walls of macropores, which are created by removal of the soft template F127 [18, 20], can be clearly observed. Meanwhile, the diameters of the macropores measured from Fig. 2b, d and f are about 242, 353, and 420 nm, respectively, which are slightly smaller than those of the silica microspheres used as the template for the macropores. This phenomenon is mainly caused by shrinkage of the macropores during the carbonization [20].

Figure 3a presents the N_2 adsorption–desorption isotherms of the HPCs. The nitrogen adsorption isotherm at 77 k for the HPCs can be classified as type IV isotherms with a hysteresis loop. The adsorption patterns at low relative pressure ($P/P_0 < 0.4$) indicate the existence of micropores, while those at higher pressures than 0.4 P/P_0 are attributed to capillary condensation of nitrogen in the mesopores and multilayer adsorption on the mesopores and macropores. The pore size distributions of the HPCs calculated from the adsorption branches of nitrogen isotherm by the BJH method are shown in Fig. 3b. All the HPCs show two sharp peaks centered at $\sim$3.0 and $\sim$10 nm, which are probably caused by the removal of phenolic resin and F127, respectively. The porous characteristics of HPCs are summarized in Table 1. With the increase in the silica microsphere diameter, the BET surface areas and pore volumes decrease, and HPC-242 exhibits the largest BET surface areas and pore volumes.

The Raman spectrum of the HPC-242 is shown in Fig. 4. There is a strong peak at 1595 cm^{-1} (G-band) and weak peak at 1350 cm^{-1} (D-band). The G-band is attributed to the vibration of sp^2-bonded carbon atoms in a two-demensional hexagonal lattice, which stands for typical graphite [22, 23], while the D-band is characteristic of the disordered or amorphous carbon. The intensity ratio of G-band (1680 a.u.) to D-band (1380 a.u.) is 1.22, indicating that the HPCs are partially composed of graphite structures [24].

Electrochemical properties

Typical cyclic voltammograms (CVs) of the prepared HPC materials were measured at a scan rate of 2 mV s^{-1} in 1 M aqueous H_2SO_4 are shown in Fig. 5a. It can be found that all HPCs exhibit quasi-rectangular CV shape, indicating their good double-layer capacitive behavior at low voltage scan rate. In addition, the responding current density of electrode materials is increased with a decrease in the size of macropores of HPCs. The largest current density response of HPC-242 implies the highest specific capacitance than that of HPC-353 and HPC-420, which is mainly due to the fastest ion transport behavior in HPC-242. Figure 5b presents the CVs of HPC-242 at different scan rates. As the scan rate is increased, the rectangular shape of CVs is maintained with only slight distortion, which demonstrates that the HPC-242 has an excellent capacitive behavior at high voltage scan rates and a small mass-transfer resistance [25]. This reveals that the hierarchical porous structure results in good capacitive behavior of HPC-242. First, the combination of different pores in HPCs can provide a harmonious electrochemical environment for the full realization of fast ion transport and high charge storage capability. Second, the electrolyte ions can be transported more smoothly and swiftly in the HPC-242 due to its larger ion-accessible surface area for charge accumulation, as compared to HPC-353 and HPC-420. Therefore, the HPC-242 shows the best electrochemical performance among the HPCs.

To further quantify their specific capacitance, galvanostatic CD curves of HPCs were measured at a current

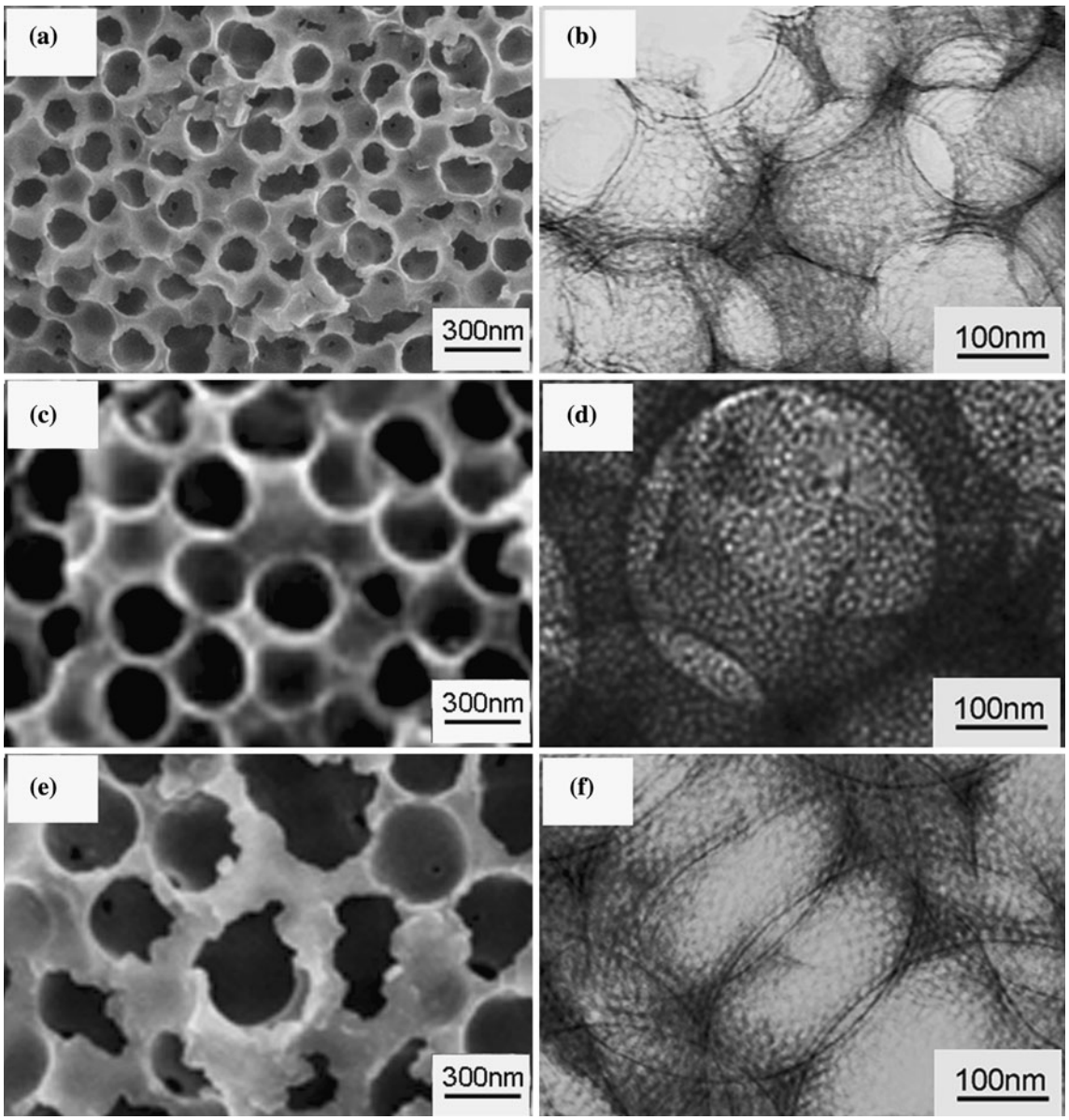

Fig. 2 SEM images of **a** HPC-242, **c** HPC-353, and **e** HPC-420; TEM images of **b** HPC-242, **d** HPC-353, and **f** HPC-420

density of 0.1 A g^{-1} as shown in Fig. 6. All profiles of CD are isosceles triangle curves, an indication of an ideal EDLC capacitor with the performance of electrochemical stability and reversibility [25]. To better understand the effects of current density and macropore size of HPCs on the electrochemical performance, the specific capacitance of HPCs at different current densities are summarized in Table 2. The specific capacitance of HPCs can be calculated according to the following equation [26, 27].

$$C_{HPC} = \frac{2(I \times t)}{m \times \Delta V} \quad (1)$$

where C_{HPC} is specific capacitance (F g^{-1}), I is the CD current (A), t is the discharge time (s), m is the mass of active material within the electrode and ΔV is the potential difference during the discharging.

Apparently, HPC-242 has supreme specific capacitance at all current densities, which is in accordance with the result of CV. Note that the specific capacitances of HPCs decrease with increasing current density. At high current density, electrolyte ions quickly transfer and do not have enough time to penetrate into the micropores, and thus cannot take full advantage of pores in the carbons; while at low current density, electrolyte ions can make full use of the hierarchical pores. However, when the current density increased to 1 A g^{-1}, over 88 % of the original capacitance of HPCs is retained due to their superior hierarchical porous structure.

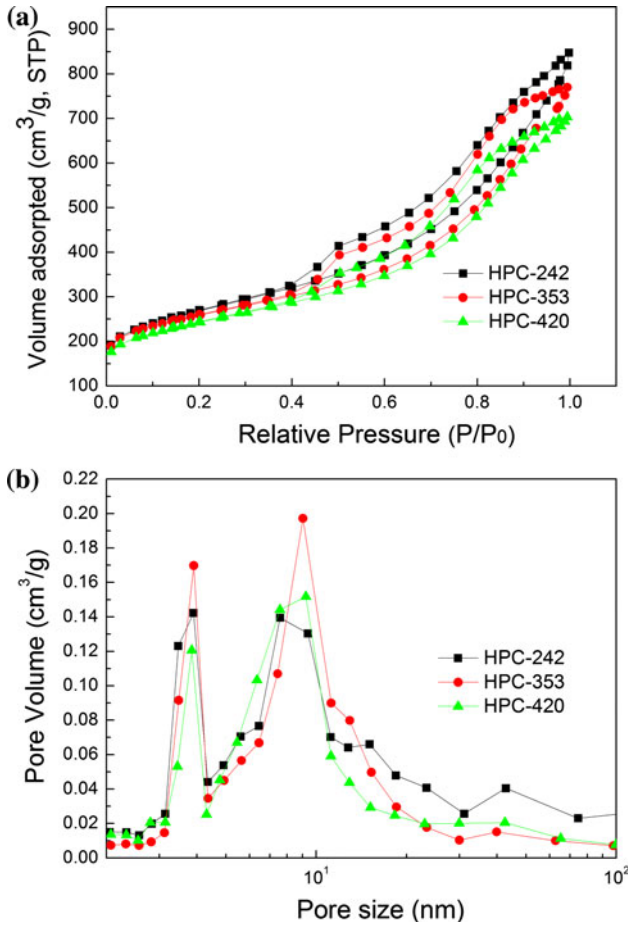

Fig. 3 **a** N_2 sorption isotherms and **b** BJH pore size distribution curves of HPCs

Table 1 Pore structure parameters of various HPCs

Sample	BET ($m^2\ g^{-1}$)	V_{total} ($cm^3\ g^{-1}$)	V_{micro} ($cm^3\ g^{-1}$)
HPC-242	940	1.2	0.33
HPC-353	898	1.1	0.4
HPC-420	845	1.04	0.37

To further investigate the influence of hierarchical porous structure on electrochemical property, electrochemical impedance measurement was employed. Figure 7 shows the impedance spectra for all HPCs. All the spectra show a depressed semicircle at the high-medium frequency and vertical lines at low frequency region. The depressed semicircle curves depict a typical electric double-layer behavior while the vertical lines reveal the supercapacitive behavior. The diameters of the semicircle reflect charge transfer resistance which is strongly dependent on the abilities of ion transfer and electron conduction [28, 29]. It can be observed that the charge transfer resistances decrease in the sequence of HPC-242 > HPC-353 > HPC-420 as revealed by the semicircle, which is in consistent

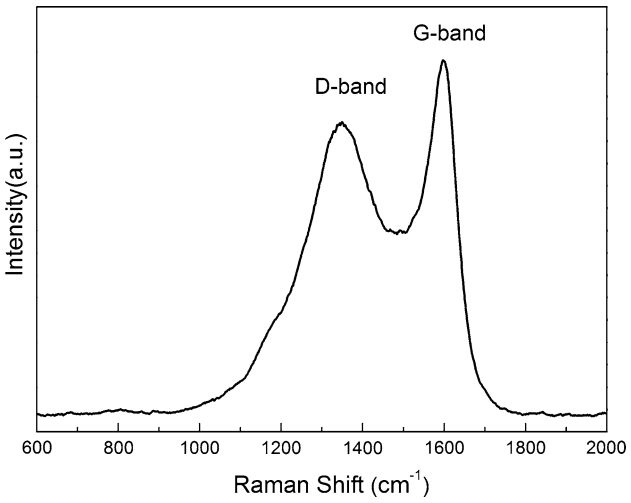

Fig. 4 Raman spectrum of HPC-242

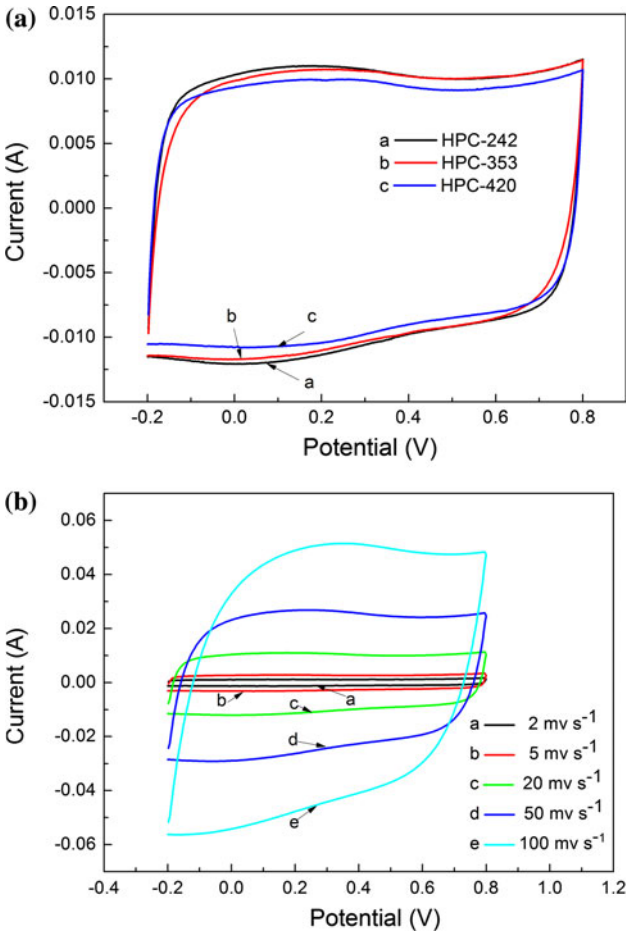

Fig. 5 **a** CVs of HPC-242, HPC-353 and HPC-420 at a scan rate of 2 mV s^{-1}. **b** CVs of HPC-242 at different scan rates

with the sequence of specific capacitances of HPCs. The lowest resistance of HPC-242 is probably caused by the smallest macropore size than others.

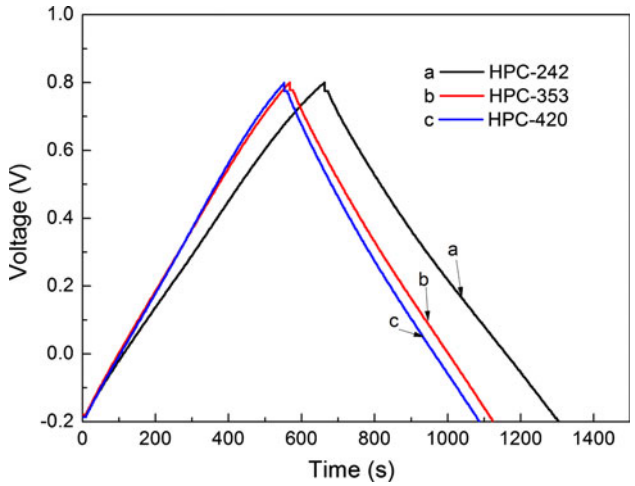

Fig. 6 Galavanostatic CD curves of HPCs

Table 2 The specific capacitance (C_{HPC}) of HPCs at different current density

Sample	C_{HPC} at different current density (A g^{-1})			
	0.1	0.2	0.5	1
HPC-242	165	156	152	146
HPC-353	150	145	142	138
HPC-420	138	134	132	129

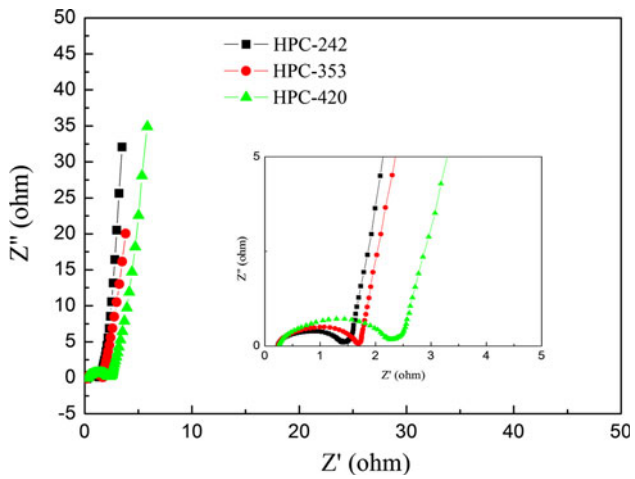

Fig. 7 Electrochemical impedance spectra of HPCs

Conclusions

In summary, HPCs with various macropore sizes (242, 353, and 420 nm) were fabricated by a facile casting method using silica microspheres as hard template, phenolic resin as carbon source, and F127 as soft template. With the increase in the silica microsphere diameter, the BET surface areas and pore volumes decreased, and HPC-242 showed the largest BET surface areas and pore volumes. As evidenced by cyclic voltammetry, galvanostatic CD, and electrochemical impedance measurements, HPC-242 exhibited a higher specific capacitance at all current density in comparison with HPC-353 and HPC-420, which is owing to its higher ion-accessible surface area. Therefore, optimal electrochemical properties of HPCs can be achieved through control of the macropore size of HPCs to provide better electrode materials for supercapacitor.

Acknowledgements This study was supported by the National Natural Science Foundation of China (20925621), the Special Projects for Nanotechnology of Shanghai (1052nm02300, 11nm0500800, 11nm0500200), the Fundamental Research Funds for the Central Universities, the Program of Shanghai Subject Chief Scientist (08XD1401500), the Shanghai Shuguang Scholars Program (10SG31), the Special Projects for Key Laboratories in Shanghai (10DZ2211100) and the project-sponsored by SRF for ROCS, SEM.

References

1. Song C, Du JP, Zhao JH, Feng SA, Du GX, Zhu ZP (2009) Chem Mater 21:1524
2. Shen WZ, Zhang SC, He Y, Li JF, Fan WB (2011) J Mater Chem 21:14036
3. Goldberg M, Landger R, Jia XQ (2007) J Biomater Sci Polym Ed 18:241
4. Lee KT, Lytle JC, Ergang NS, Oh SM, Stein A (2005) Adv Funct Mater 15:547
5. Simon P, Gogotsi Y (2008) Nat Mater 7:845
6. Li LX, Song HH, Zhang QC, Yao JY, Chen XH (2009) J Power Sources 187:268
7. Ko JM, Song RY, Yu HJ, Yoon JW, Min BG, Kim DW (2004) Electrochim Acta 50:873
8. Tamai H, Hakoda M, Shiono T, Yasuda H (2007) J Mater Sci 42:1293. doi:10.1007/s10853-006-1059-7
9. Yang S, Kim IJ, Jeon MJ, Kim K, Moon SI, Kim HS, An KH (2008) J Ind Eng Chem 14:365
10. Nam HS, Kwon JS, Kim KM, Ko JM, Kim JD (2010) Electrochim Acta 55:7443
11. Wang DW, Li F, Fang HT, Liu M, Lu GQ, Cheng HM (2006) J Phys Chem B 110:8570
12. Rolison DR (2003) Science 299:1698
13. Xing W, Qiao SZ, Ding RG, Li F, Lu GQ, Yan ZF, Cheng HM (2006) Carbon 44:216
14. Morishita T, Soneda Y, Tsumura T, Inagaki M (2006) Carbon 44:2360
15. Filho CA, Zarbin AJ (2006) Carbon 44:2869
16. Wang DW, Li F, Liu M, Lu GQ, Cheng HM (2008) Angew Chem 120:379
17. Fang BZ, Kim M, Kim JH, Yu JS (2008) Langmuir 24:12068
18. Zhao Y, Zheng MB, Cao JM, Ke XF, Liu JS, Chen YP, Tao J (2008) Mater Lett 62:548
19. Zarbin AJ, Bertholdo R, Oliveira MA (2002) Carbon 40:2413
20. Deng YH, Liu C, Yu T, Liu F, Zhang FQ, Wan Y, Zhang LJ, Wang CC, Tu B, Webley P, Wang HT, Zhao DY (2007) Chem Mater 19:3271
21. Zeng QC, Wu DC, Zou C, Xu F, Fu RW, Li ZH, Liang Y, Su DS (2010) Chem Commun 46:5927
22. Tuinsta F, Koenig J (1970) J Chem Phys 53:1126
23. Sadezky A, Muckenhuber H, Grothe H, Niessner R, Pöschl U (2005) Carbon 43:1731

24. Zhao JZ, Cheng FY, Yi CH, Liang J, Tao ZL, Chen J (2009) J Mater Chem 19:4108
25. Xing W, Huang CC, Zhuo SP, Yuan X, Wang GQ, Jurcakova DH, Yan ZF, Lu GQ (2006) Carbon 44:216
26. Qu DY, Shi H (1998) J Power Sources 74:99
27. Wang YG, Li HQ, Xia YY (2006) Adv Mater 18:2619
28. Sun GW, Wang JT, Liu XJ, Long DH, Qiao WM, Ling LC (2010) J Phys Chem C 114:18745
29. Sugimoto W, Iwata H, Yokoshima K, Murakami Y, Takasu Y (2005) J Phys Chem B 109:7330